Letter

Radiative heat exchange driven by acoustic vibration modes between two solids at the atomic scale

M. Gómez Viloria,[1] Y. Guo,[2] S. Merabia,[2] R. Messina,[1] and P. Ben-Abdallah[1,*]

[1]*Laboratoire Charles Fabry, UMR 8501, Institut d'Optique, CNRS, Université Paris-Saclay, 2 Avenue Augustin Fresnel, 91127 Palaiseau Cedex, France*

[2]*Institut Lumière Matière, Université Claude Bernard Lyon 1, CNRS, Université de Lyon, 69622 Villeurbanne, France*

(Received 1 February 2023; revised 24 August 2023; accepted 31 October 2023; published 15 November 2023; corrected 1 December 2023)

When two solids are separated by a vacuum gap of thickness smaller than the wavelength of acoustic phonons, the latter can tunnel across the gap thanks to van der Waals forces or electrostatic interactions. Here we show that these mechanical vibration modes can also contribute significantly, at the atomic scale, to the nonlocal radiative response of polar materials. By combining molecular-dynamics simulations with fluctuational-electrodynamics theory, we investigate the near-field radiative heat transfer between two slabs due to this optomechanical coupling and highlight its dominant role at cryogenic temperatures. These results pave the way to exciting avenues for the control of heat flux and the development of cooling strategies at the atomic scale.

DOI: 10.1103/PhysRevB.108.L201402

The physics of heat transfer between two solids separated by a vacuum gap in the transition regime between conduction and radiation today remains largely unknown. When solids are separated by gaps having thicknesses of tens of nanometers or more heat transfer is exclusively driven by photon exchange. In the far-field regime (distances larger than the thermal wavelength, around 10 μm at ambient temperature), this transfer is limited by Stefan-Boltzmann's law defining the blackbody limit [1]. At subwavelength scale and down to distances of about ten nanometers, the heat flux exchanged between the solids can overcome this limit by several orders of magnitude [2–12] thanks to the tunneling of evanescent photons which superimposes to the flux driven by propagative photons. Below this separation distance, heat transfer can be mediated by multiple carriers [13–17]. More specifically, at subnanometer scale, acoustic vibration modes of solids participate in the transfer. In 2015, Chiloyan *et al.* highlighted [18], by means of atomistic simulations, the dominant role played by these modes on the transfer between polar materials. In that work, it was claimed that this transfer results from the tunneling of vibration modes thanks to surface forces. Such a transfer has been described theoretically in the continuum limit for isotropic media by Pendry *et al.* [19] (see also Refs. [20,21]) using the classical elasticity theory. More recently, this description has been extended to anisotropic piezoelectric materials [22]. In this Letter, we show that acoustic vibration modes, which are traditionally purely mechanical modes in the long-wavelength (LW) limit, are not only able to tunnel through the separation gap thanks to the surface forces existing between the two solids but also contribute, at atomic-scale separation distances (i.e., short wavelengths limit), to the nonlocal radiative response of materials. In the LW limit, it is well-known that the optical phonons are the only excitations that give rise to local electric dipole moments inside the material, owing to the motion of neighboring atoms with opposite partial charges in opposite directions. In this limit, the optical phonons are the only link between the atomic vibrations within the solid and the surrounding electromagnetic field. These optical vibration modes entirely drive the radiative response of material. Although a mesoscopic theory describing the nonlocal response of polar materials has been recently introduced [23] in an analogous way as the hydrodynamic description of electron gas in nonlocal plasmonics [24,25], this theory suffers from a fundamental limitation to properly describe light-matter interactions at the atomic scale. Indeed, it ignores the crucial role played by the acoustic vibration modes in the radiative response of material. However, as we will see, at the atomic scale, acoustic vibration modes play a major role in this response. Here, we make a detailed description of this optomechanical coupling and we highlight its importance in the radiative heat exchanges between two solids close to the physical contact. We demonstrate that, contrary to wide belief, these acoustic vibration modes can significantly contribute to the radiative heat exchanges and can even be dominant, in front of the contribution coming from optical phonons, in the cryogenic regime.

To start, let us consider a polar material of arbitrary crystalline structure. To describe light interaction with this crystal in the infrared frequency range and at atomic-scale separation distances, a nonlocal model of the radiative response of the material must be introduced. To go beyond the Gubbin and De Liberato theory [23], a fully atomistic calculation of the dielectric response has been performed (see Supplemental Material [26] and Refs. [27–30] therein), based on the analysis of the fluctuations of the polarization density within the crystal. In spatially invariant crystals, this density is related to local electric field $\mathbf{E}(\mathbf{r}, t)$ through the nonlocal relation (assuming the system stationary)

$$\mathbf{P}(\mathbf{r}, t) = \epsilon_0 \iint \mathrm{d}\mathbf{r}'\mathrm{d}t' \ \overleftrightarrow{\chi}(\mathbf{r} - \mathbf{r}', t - t') \cdot \mathbf{E}(\mathbf{r}', t'), \quad (1)$$

*pba@institutoptique.fr

where ϵ_0 is the vacuum permittivity, whereas $\overleftrightarrow{\chi}(\mathbf{r}-\mathbf{r}', t-t')$ denotes the electric susceptibility tensor of the crystal, $\mathbf{r}-\mathbf{r}'$ and $t-t'$ being the spatial and temporal distance, respectively, between polarization and electric field. According to the fluctuation-dissipation theorem [31], the spatial Fourier components of the susceptibility tensor at temperature T read

$$\chi_{mn}(\mathbf{k}, t) = -H(t)\frac{1}{\epsilon_0 k_B T}\frac{\mathrm{d}}{\mathrm{d}t}\langle \delta P_m(\mathbf{k}, 0)\delta P_n^*(\mathbf{k}, t)\rangle, \quad (2)$$

where $\delta P_m = P_m - \langle P_m\rangle$, $\langle . \rangle$ denotes an ensemble average, $*$ is the conjugation operation, and H is the Heaviside function. For a statistically stationary process (i.e., $\mathrm{d}\langle P_m\rangle/\mathrm{d}t = 0$) we have, equivalently,

$$\chi_{mn}(\mathbf{k}, t) = -H(t)\frac{1}{\epsilon_0 k_B T}\frac{\mathrm{d}}{\mathrm{d}t}\langle P_m(\mathbf{k}, 0)P_n^*(\mathbf{k}, t)\rangle. \quad (3)$$

It turns out by time Fourier transformation of this expression that the electric susceptibility and the relative dielectric permittivity of the crystal read

$$\chi_{mn}(\mathbf{k}, \omega) = \frac{1}{\epsilon_0 k_B T}\left[\langle P_m(\mathbf{k}, 0)P_n^*(\mathbf{k}, 0)\rangle + \mathrm{i}\omega\int_0^\infty \mathrm{d}t\ e^{\mathrm{i}\omega t}\langle P_m(\mathbf{k}, 0)P_n^*(\mathbf{k}, t)\rangle\right] \quad (4)$$

and $\epsilon_{mn}(\mathbf{k}, \omega) = \chi_{mn}(\mathbf{k}, \omega) + \delta_{mn}$, respectively; δ_{mn} being the Kronecker delta. These expressions relate the nonlocal radiative response of material to the correlations functions of local dipolar moments. The latter are, in turn, related to the motion of partial charges which are associated to each atom. In contrast, we define the local response as the limit $\chi_{mn}(\mathbf{k}, \omega) \to \chi_{mn}(\mathbf{k} = 0, \omega)$ valid for large separation distances. Equation (4) can be generalized to the quantum regime by relating the correlation function of fluctuating polarization density operator to the electrical susceptibility through the general Kubo formula [32].

To give insight into the link between the vibration modes and the radiative response of material, we detail below the case of the diatomic chain [33] which is the simplest polar crystal. In this particular case, it is well-known that the dispersion relation of resonant modes reads

$$\omega^2 = C\left(\frac{1}{M_1}+\frac{1}{M_2}\right) \pm C\left[\left(\frac{1}{M_1}+\frac{1}{M_2}\right)^2 - \frac{4\sin^2(ka/2)}{M_1 M_2}\right]^{1/2}, \quad (5)$$

where C denotes the chain stiffness between the atoms of mass M_1 and M_2 while a is the lattice period and k is the mode wave number. As for the amplitudes $u_l = u_k \exp(\mathrm{i}[kla - \omega t])$ and $v_l = v_k \exp(\mathrm{i}[kla - \omega t])$ of the normal modes associated with the masses M_1 and M_2, respectively, in the unit cell l they satisfy the relation

$$\frac{u_k}{v_k} = \frac{2Ce^{-\mathrm{i}ka/2}\cos(ka/2)}{2C - M_1\omega^2}. \quad (6)$$

In the LW limit ($k \to 0$), the dispersion relation of optical (high frequency) and acoustic (low frequency) branches read

$$\omega^2 = 2C\left(\frac{1}{M_1}+\frac{1}{M_2}\right), \quad \omega^2 = \frac{C}{2(M_1+M_2)}(ka)^2, \quad (7)$$

and the amplitudes of optical and acoustic normal modes satisfy, respectively, the relations $u_k/v_k \approx -M_2/M_1$ (i.e., out-of-phase atomic vibration) and $u_k/v_k \approx 1$ (i.e., in-phase atomic vibration), showing that only the optical modes give rise to dipole moments. On the other hand, close to the upper bound of the Brillouin zone (i.e., $k \approx \pi/a$), that is, in the extreme near-field regime, the situation radically changes. As shown in Fig. 1(a), an anticrossing of acoustic and optical branches appears in this zone, showing a strong coupling between these modes with a frequency splitting (assuming here $M_2 < M_1$) $\Gamma = \omega_\mathrm{o} - \omega_\mathrm{a}$, with $\omega_\mathrm{o} = \sqrt{2C/M_2}$ and $\omega_\mathrm{a} = \sqrt{2C/M_1}$. As far as the amplitudes of normal modes are concerned, we see from the general expression Eq. (6) that

$$\frac{u_k}{v_k} \approx \frac{\mathrm{i}C(ka-\pi)}{2C - M_1\omega_{\mathrm{o,a}}^2}, \quad (8)$$

so $u_k/v_k \to 0$ for the optical modes and $u_k/v_k \to \infty$ for the acoustic modes. These relations demonstrate that both types of modes give rise to dipole moments and therefore both contribute to the radiative response of the chain. Moreover, these relations also demonstrate that for both acoustic and optical modes, one atom is motionless in the unit cell while the second is free to oscillate making these modes identical in nature.

The radiative contribution of acoustic modes to the nonlocal radiative response can be directly observed in a concrete scenario. In Fig. 1(b), we show the dielectric response of a magnesium oxide (MgO) crystal in the (001) axis of reciprocal space obtained by molecular-dynamics simulation [26]. This material has been chosen to get well-separated optical and acoustic branches, making the analysis and interpretation of results easier. The comparison of this mapping with the dispersion relations of resonant vibration modes [Fig. 1(c)] calculated by solving the secular equation of the crystal clearly shows the contribution of optical branches at high frequencies but also the one of acoustic branches at low frequencies. We also observe, at the edge of the Brillouin zone, the anticrossing, previously mentioned for the diatomic chain, between the longitudinal optical (LO) and longitudinal acoustic (LA) branches, true signature of strong coupling between these vibration modes in this region. It is worthwhile to note that the contribution of acoustic modes is not limited to the edge of the Brillouin zone. In Fig. 1(b), we see that the acoustic mode can couple to the electromagnetic field relatively far away from this region. For MgO, the contribution of acoustic modes to the nonlocal response of crystal can be observed down to wave vectors $k \approx 1/2a$; $a = 4.2$ Å being the lattice constant of crystal.

The role played by these modes on the radiative heat transfer can then be investigated thanks to fluctational-electrodynamics theory. According to this framework, the conductance of radiative heat exchanged at temperature T between two solids separated by a vacuum gap of thickness

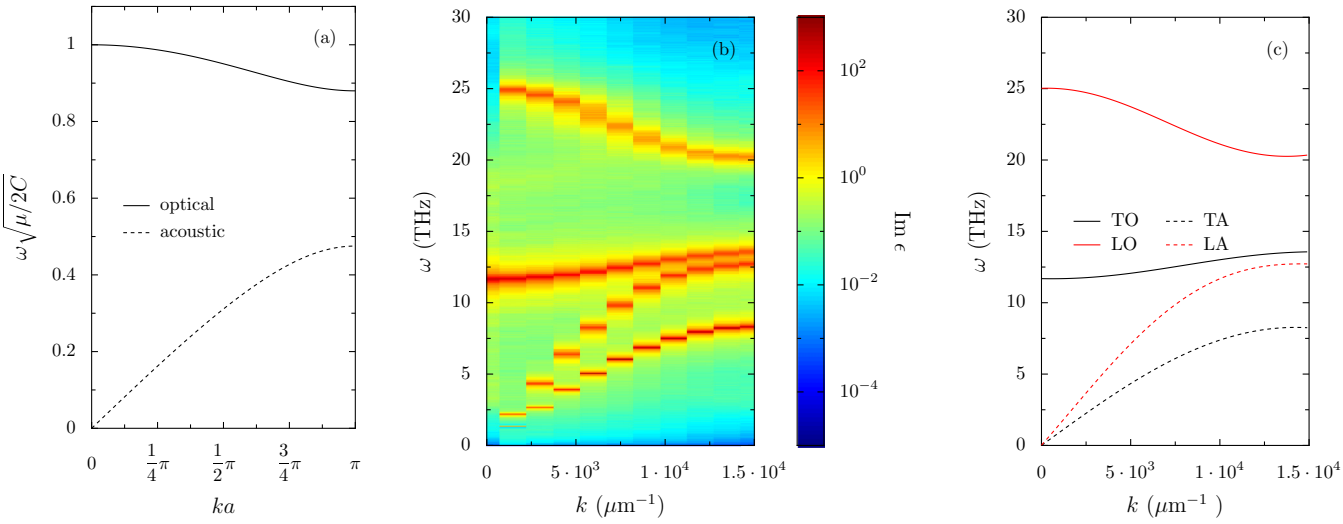

FIG. 1. (a) Dispersion relation of eigenmodes in a diatomic chain with a reduced mass $\mu = \frac{M_1 M_2}{M_1+M_2}$, chain stiffness C, and lattice constant a. (b) Imaginary part of the dielectric permittivity of a MgO cubic crystal (bulk) in the (001) direction of reciprocal space, calculated by molecular dynamics. (c) Dispersion relation of eigenmodes in the MgO crystal obtained by solving its secular equation. The four eigenmodes are known as the longitudinal optical (LO; solid red), transverse optical (TO; solid black), longitudinal acoustic (LA; dashed red) and transverse acoustic (TA; dashed black) branches.

d can be written in the Landauer-like form [3,34,35]

$$G(T,d) = \int_0^\infty \frac{\mathrm{d}\omega}{2\pi}\frac{\mathrm{d}\Theta}{\mathrm{d}T}(\omega,T)\int\frac{\mathrm{d}\boldsymbol{\kappa}}{(2\pi)^2}\sum_{\alpha=\mathrm{s,p}}\mathcal{T}_\alpha(\kappa,\omega,d), \tag{9}$$

where $\Theta(\omega,T) = \hbar\omega/[\exp(\hbar\omega/k_\mathrm{B}T)-1]$ is the mean energy of the Planck oscillator at temperature T and $\mathcal{T}_\alpha(\kappa,\omega,d)$ is the transmission coefficient in polarization $\alpha \in \{\mathrm{s,p}\}$ of mode (κ,ω), κ being the parallel component of the wave vector. Assuming a system with azimuthal symmetry, this coefficient reads

$$\mathcal{T}_\alpha(\kappa,\omega,d) = \begin{cases} \frac{(1-|r_{\alpha,1}|^2)(1-|r_{\alpha,2}|^2)}{|1-r_{\alpha,1}r_{\alpha,2}\exp[2\mathrm{i}k_z d]|^2}, & \kappa < \omega/c \\ \frac{4\,\mathrm{Im}\,r_{\alpha,1}\,\mathrm{Im}\,r_{\alpha,2}\exp[-2\,\mathrm{Im}\,(k_z)d]}{|1-r_{\alpha,1}r_{\alpha,2}\exp[-2\,\mathrm{Im}\,(k_z)d]|^2}, & \kappa \geqslant \omega/c. \end{cases} \tag{10}$$

Here, $r_{\alpha,i}$ denotes the reflection coefficient of medium $i = 1, 2$ from vacuum and $k_z = \sqrt{(\omega/c)^2-\kappa^2}$ is the normal component of wave vector in vacuum while $\kappa = |\boldsymbol{\kappa}|$. The reflection coefficients can be written in terms of surface impedances $Z_{\alpha,i}$ as follows [36]:

$$r_{\mathrm{s},i}(\kappa,\omega) = \frac{Z_{\mathrm{s},i}(\kappa,\omega)-\frac{\omega}{c^2 k_z}}{Z_{\mathrm{s},i}(\kappa,\omega)+\frac{\omega}{c^2 k_z}}, \tag{11a}$$

$$r_{\mathrm{p},i}(\kappa,\omega) = \frac{\frac{k_z}{\omega}-Z_{\mathrm{p},i}(\kappa,\omega)}{\frac{k_z}{\omega}+Z_{\mathrm{p},i}(\kappa,\omega)}, \tag{11b}$$

with [37]

$$Z_{\mathrm{s},i}(\kappa,\omega) = \frac{2\mathrm{i}}{\pi\omega}\int_0^\infty \frac{\mathrm{d}q_z}{\epsilon_{\mathrm{t},i}(k,\omega)-(ck/\omega)^2}, \tag{12a}$$

$$Z_{\mathrm{p},i}(\kappa,\omega) = \frac{2\mathrm{i}}{\pi\omega}\int_0^\infty \frac{\mathrm{d}q_z}{k^2}\left[\frac{q_z^2}{\epsilon_{\mathrm{t},i}(k,\omega)-(ck/\omega)^2}+\frac{\kappa^2}{\epsilon_{\mathrm{l},i}(k,\omega)}\right], \tag{12b}$$

where $k^2 = q_z^2+\kappa^2$. Here $\epsilon_{\mathrm{l},i}(k,\omega)$ and $\epsilon_{\mathrm{t},i}(k,\omega)$, denote the longitudinal and transverse dielectric functions which are calculated by molecular-dynamics simulations [26]. The computed spectra of heat conductances calculated from the integrand over the ω integral of Eq. (9) with the nonlocal response of material (dependent on wave vector k) for different separation distances and different temperatures are presented in Figs. 2(a) and 2(b) and compared with conductances calculated with the local dielectric permittivity $\epsilon(\omega)$ (independent of k).

At gaps $d > 1$ nm, we see that the heat transfer mainly stems from modes at high frequencies. The comparison of spectra with the dielectric permittivity plotted in Fig. 1 shows that these modes are in the spectral range of optical phonons. However, below this critical distance we observe that the lower-frequency modes also participate in the transfer. We also note in Fig. 2(b) that the relative weight of these modes in comparison with the high-frequency modes increases at low temperature. These modes even become dominant in the cryogenic regime ($T < 100$ K). The inspection of the transmission coefficients plotted in Fig. 3 clearly shows that these low-frequency modes correspond to acoustic vibration modes. This result unquestionably demonstrates that the acoustic modes contribute radiatively to the transfer at small separation distances. Unlike the conductivelike heat transfer due to the mechanical tunneling of acoustic modes mediated by van der Waals forces between the two solids, this transfer is purely radiative and is related to dipole-dipole interactions induced by the acoustic vibration modes. Also, it must be noted [see Fig. 1(b)] that the acoustic modes with very small wave vector do not play any role in the radiative response of the material. These modes can in principle participate to the heat transfer by tunneling but not to the radiative one. However, as shown in Ref. [18], this tunneling is negligible because of the weakness of surface forces.

Finally, we analyze the ratio of the nonlocal radiative conductance to the local one. The results plotted in Fig. 4 with respect to the separation distance for different temperatures

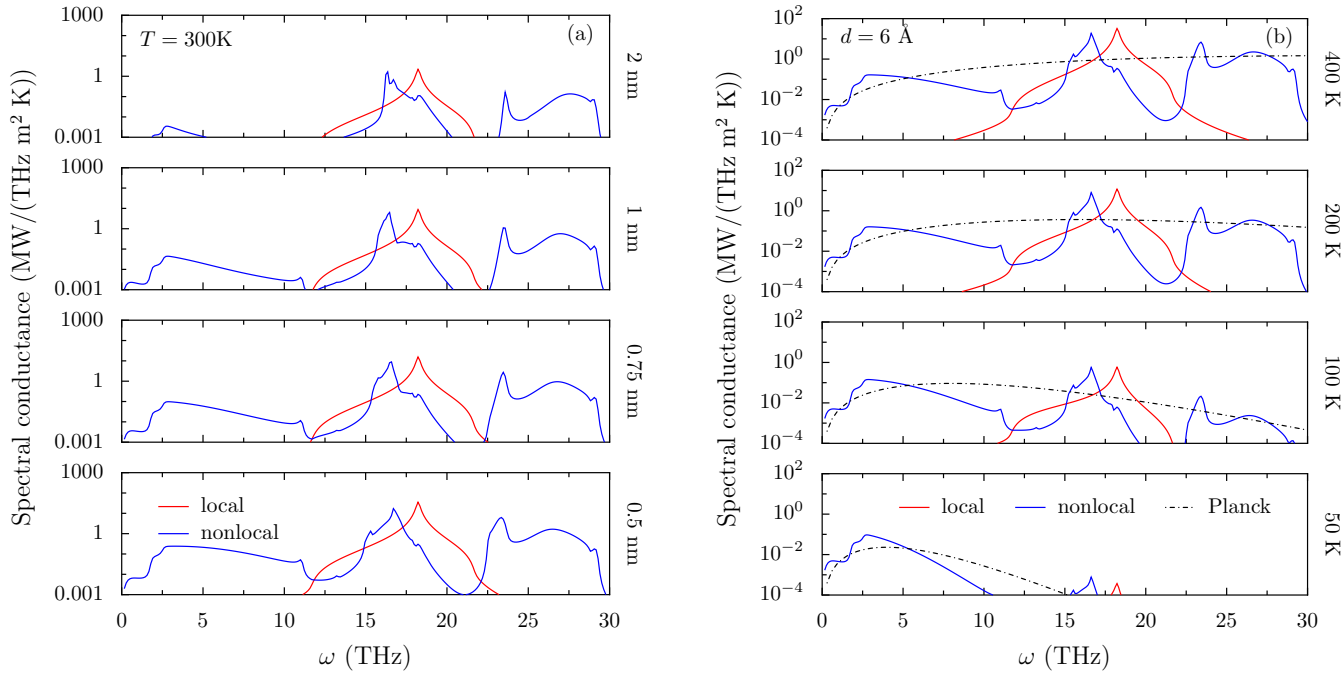

FIG. 2. Thermal conductance spectra between two MgO samples for different separation distances at (a) $T = 300$ K and (b) for different temperatures at $d = 6$ Å. The conductance is calculated using both the local (red) and nonlocal (blue) dielectric response of material. The dash-dotted curves represent Planck's law in arbitrary units.

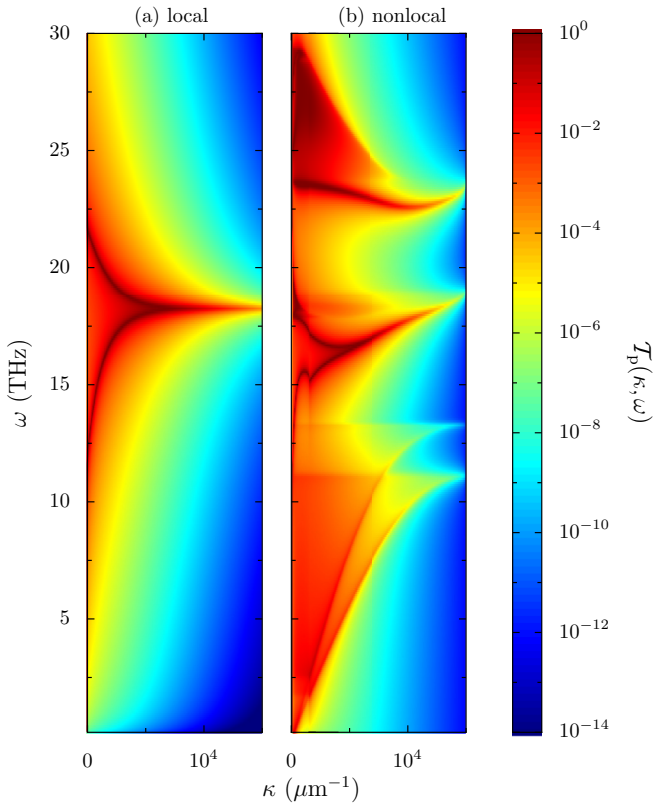

FIG. 3. Local (left) and nonlocal (right) transmission coefficient of p-polarized radiative heat exchange between two MgO samples separated by a vacuum gap of $d = 6$ Å.

show, at large distance, that the local and nonlocal conductances become, as expected, identical. Moreover, we note that nonlocal effects dominate at low temperature, in the cryogenic regime owing to the dipoles generated by the acoustic vibration modes. This result would be trivial if these modes were known to give rise to electric dipoles. But this is not generally the case for small wave vectors. Hence, at relatively large distances [see Fig. 2(a)], these modes do not contribute to the transfer. On the other hand, at close separation distance (large wave vectors), this is not true anymore and these mechanical vibration modes contribute significantly to the heat transfer, this contribution being purely radiative in nature. In the inset of Fig. 4 we see at ambient temperature that the conductance

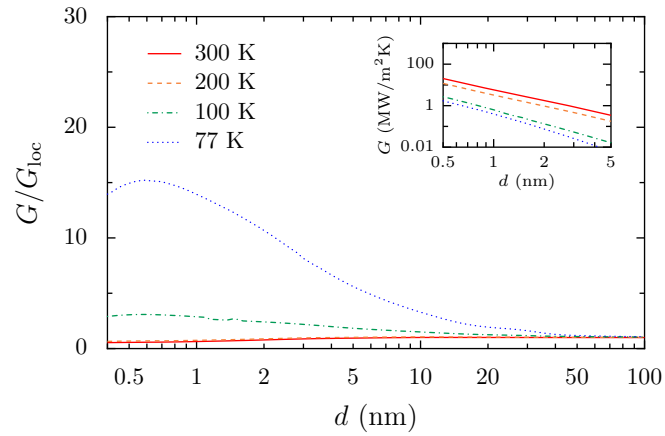

FIG. 4. Nonlocal vs local radiative conductance with respect to the separation distance for different temperatures. Inset: Full radiative conductance with respect to the separation distance.

follows the usual power-law scaling in $1/d^2$, d being the separation gap between the two plates (see Ref. [26]). On the the other hand, in the cryogenic regime, the scaling changes since the transfer is not mediated anymore by the surface phonon-polaritons.

In this Letter, we shed light on the radiative heat transfer between polar materials close to the physical contact. We have shown that the acoustic vibration modes play a major role in the nonlocal radiative response of material and even become the dominant channel for radiative heat exchanges at the atomic scale in the cryogenic regime. Since the acoustic vibration modes can be excited with the help of piezoelectric transducers or using Raman or Brillouin light scattering, the radiative heat exchanges could, in principle, be actively tuned at the atomic scale. Future developments in this direction will certainly benefit from recent progress in instrumental optomechanics [38].

This research was supported by the French Agence Nationale de la Recherche (ANR) under Grant No. ANR-20-CE05-0021-01 (NearHeat).

[1] M. Planck, *The Theory of Heat Radiation* (Forgotten Books, Leipzig, 2010).
[2] S. M. Rytov, *Theory of Electrical Fluctuations and Thermal Radiation* (Academy of Sciences Press of USSR, Moscow, 1953).
[3] D. Polder and M. Van Hove, Phys. Rev. B **4**, 3303 (1971).
[4] K. Joulain, J.-P. Mulet, F. Marquier, R. Carminati, and J.-J. Greffet, Surf. Sci. Rep. **57**, 59 (2005).
[5] A. I. Volokitin and B. N. J. Persson, Rev. Mod. Phys. **79**, 1291 (2007).
[6] S.-A. Biehs, R. Messina, P. S. Venkataram, A. W. Rodriguez, J. C. Cuevas, and P. Ben-Abdallah, Rev. Mod. Phys. **93**, 025009 (2021).
[7] C. Hargreaves, Phys. Lett. A **30**, 491 (1969).
[8] A. Narayanaswamy, S. Shen, and G. Chen, Phys. Rev. B **78**, 115303 (2008).
[9] S. Shen, A. Narayanaswamy, and G. Chen, Nano Lett. **9**, 2909 (2009).
[10] E. Rousseau, A. Siria, G. Joudran, S. Volz, F. Comin, J. Chevrier, and J.-J. Greffet, Nat. Photon. **3**, 514 (2009).
[11] R. S. Ottens, V. Quetschke, S. Wise, A. A. Alemi, R. Lundock, G. Mueller, D. H. Reitze, D. B. Tanner, and B. F. Whiting, Phys. Rev. Lett. **107**, 014301 (2011).
[12] T. Kralik, P. Hanzelka, M. Zobac, V. Musilova, T. Fort, and M. Horak, Phys. Rev. Lett. **109**, 224302 (2012).
[13] R. Messina, S.-A. Biehs, T. Ziehm, A. Kittel, and P. Ben-Abdallah, arXiv:1810.02628.
[14] T. Tokunaga, A. Jarzembski, T. Shiga, K. Park, and M. Francoeur, Phys. Rev. B **104**, 125404 (2021).
[15] T. Tokunaga, M. Arai, K. Kobayashi, W. Hayami, S. Suehara, T. Shiga, K. Park, and M. Francoeur, Phys. Rev. B **105**, 045410 (2022).
[16] Y. Guo, C. Adessi, M. Cobian, and S. Merabia, Phys. Rev. B **106**, 085403 (2022).
[17] M. Gómez Viloria, Y. Guo, S. Merabia, P. Ben-Abdallah, and R. Messina, Phys. Rev. B **107**, 125414 (2023).
[18] V. Chiloyan, J. Garg, K. Esfarjani, and G. Chen, Nat. Commun. **6**, 6755 (2015).
[19] J. B. Pendry, K. Sasihithlu, and R. V. Craster, Phys. Rev. B **94**, 075414 (2016).
[20] A. I. Volokitin, JETP Lett. **109**, 749 (2019).
[21] A. I. Volokitin, J. Phys.: Condens. Matter **32**, 215001 (2020).
[22] Z. Geng and I. J. Maasilta, Phys. Rev. Res. **4**, 033073 (2022).
[23] C. R. Gubbin and S. De Liberato, Phys. Rev. X **10**, 021027 (2020).
[24] R. Fuchs and K. L. Kliewer, Phys. Rev. B **3**, 2270 (1971).
[25] C. Cirací, J. B. Pendry, and D. R. Smith, ChemPhysChem **14**, 1109 (2013).
[26] See Supplemental Material at http://link.aps.org/supplemental/10.1103/PhysRevB.108.L201402 for details on the calculations of the dielectric function of MgO and on the physical origin of the dipolar response induced by the acoustic vibration modes.
[27] A. P. Thompson, H. M. Aktulga, R. Berger, D. S. Bolintineanu, W. M. Brown, P. S. Crozier, P. J. in't Veld, A. Kohlmeyer, S. G. Moore, and T. D. Nguyen, Comput. Phys. Commun. **271**, 108171 (2022).
[28] M. Matsui, J. Chem. Phys. **91**, 489 (1989).
[29] Y. Chalopin, M. Hayoun, S. Volz, and H. Dammak, Appl. Phys. Lett. **104**, 011905 (2014).
[30] H. B. Callen and T. A. Welton, Phys. Rev. **83**, 34 (1951).
[31] D. Chandler, *Introduction to Modern Statistical Mechanics* (Oxford University Press, New York, 1987).
[32] R. Zwanzig, Annu. Rev. Phys. Chem. **16**, 67 (1965).
[33] C. Kittel, *Introduction to Solid State Physics* (John Wiley and Sons, River Street, Hoboken, NJ, 2005).
[34] P. Ben-Abdallah and K. Joulain, Phys. Rev. B **82**, 121419(R) (2010).
[35] S.A. Biehs, E. Rousseau, and J. J. Greffet, Phys. Rev. Lett. **105**, 234301 (2010).
[36] G. W. Ford and W. H. Weber, Phys. Rep. **113**, 195 (1984).
[37] R. Esquivel and V. B. Svetovoy, Phys. Rev. A **69**, 062102 (2004).
[38] R. C. Ng, A. El Sachat, F. Cespedes, M. Poblet, G. Madiot, J. Jaramillo-Fernandez, O. Florez, P. Xiao, M. Sledzinska *et al.*, Nanoscale **14**, 13428 (2022).

Correction: Information regarding the curves in Figure 1 appeared erroneously as the last sentence of the Figure 2 caption and has been moved to the Figure 1 caption. A minor labeling error in the Figure 2 caption has been fixed.